

Research article

Alexey V. Krasavin^{a,*}, Pan Wang^a, Mazhar E. Nasir, Yunlu Jiang and Anatoly V. Zayats*

Tunneling-induced broadband and tunable optical emission from plasmonic nanorod metamaterials

<https://doi.org/10.1515/nanoph-2019-0411>

Received October 7, 2019; revised December 25, 2019; accepted December 31, 2019

Abstract: We demonstrate a metamaterial platform for electrically driven broadband light emission induced by electron tunneling. Both the Fabry-Perot and waveguided modes of the metamaterial slab as well the plasmonic mode of the tunneling gap are identified as contributing to shaping the emission spectrum. This opens up an opportunity to design the spectrum and polarization of the emitted light by tuning the metamaterial modes via the geometric parameters of the nanostructure throughout the visible and near-infrared spectral ranges. The efficient coupling of the tunneling-induced emission to the waveguided modes is beneficial for the development of integrated incoherent light sources, while the outcoupled emission provides a source of free-space radiation. The demonstrated incoherent nanoscale light sources may find applications in the development of integrated optoelectronic circuits, optical sensing platforms, imaging, and metrology.

Keywords: plasmonics; metamaterials; electron tunneling; nanoscale light sources.

1 Introduction

Nanophotonic approaches, which provide strongly confined light in waveguides or nanoparticles, are attractive for a broad range of applications in integrated optoelectronic circuits, bio- and chemical sensing, nonlinear optics, data storage, and quantum technologies, to name but a few [1–3]. In many cases, external laser illumination through bulky lenses, prisms, gratings, or fibers is used to provide input signals in nanophotonic devices, such as Si or plasmonic waveguides, and to pump nanolasers and sensing transducers. At the same time, a requirement to develop integrated electrically driven nano- and microlasers for the nanophotonic circuitry has led to several demonstrations of integration of III-V heterogeneous lasers in Si waveguides [4, 5] and vertical-cavity surface-emitting lasers in plasmonic waveguides [6], as well as stand-alone electrically pumped nanolasers [7]. The former two are difficult to scale down due to the requirements of coupling gratings to redirect light, while the latter is challenging to integrate on a chip. In many cases, however, unless coherent signal processing is a requirement, incoherent electrically driven nanoscale light sources would be sufficient for most applications. The integration of such light-emitting diodes has been demonstrated for direct excitation of surface plasmon polaritons in a metal-insulator-metal (MIM) waveguide [8], but still requires tedious incorporation of semiconducting or polymer components in the plasmonic circuitry.

Recently, inspired by the well-known effect of light generation in a tunneling junction of a scanning tunneling microscope [9], inelastic tunneling of electrons in plasmonic tunnel junctions has been demonstrated as a promising method for direct electric excitation of plasmons and photons, which has the advantage of an ultra-small footprint [10–13]. By engineering the geometry of the junctions, an external quantum efficiency has been optimized to achieve values around 2% [13]. The integration of such nanoscale electrically driven optical sources into nanophotonic circuitry is the next step.

In this paper, we make use of the principle of nanoscale light sources excited by tunneling of electrons to demonstrate their direct coupling to the electromagnetic

^aAlexey V. Krasavin and Pan Wang: These authors contributed equally to this work.

*Corresponding authors: Alexey V. Krasavin and Anatoly V. Zayats, Department of Physics and London Centre for Nanotechnology, King's College London, Strand, London WC2R 2LS, UK, e-mail: alexey.krasavin@kcl.ac.uk. <https://orcid.org/0000-0003-2522-5735> (A.V. Krasavin); a.zayats@kcl.ac.uk (A.V. Zayats)

Pan Wang: Department of Physics and London Centre for Nanotechnology, King's College London, Strand, London WC2R 2LS, UK; and State Key Laboratory of Modern Optical Instrumentation, College of Optical Science and Engineering, Zhejiang University, Hangzhou 310027, China

Mazhar E. Nasir and Yunlu Jiang: Department of Physics and London Centre for Nanotechnology, King's College London, Strand, London WC2R 2LS, UK

modes supported by a metamaterial device. Coupling to these modes shapes the spectrum of the emission from the tunnel junction and also controls the quantum yield. We considered hyperbolic metamaterials based on plasmonic nanorods aligned perpendicular to the substrate, which have already shown great potential for achieving arrays of nanoscale light sources, also opening opportunities for the realization of hot-electron-driven nanoreactors and artificial synapses for artificial neural networks [12, 14]. Due to the strong near-field coupling between plasmonic nanorods in the assembly, the plasmonic nanorod metamaterials possess unique optical properties, which have already led to the demonstration of practical applications, such as bio- and chemical sensing [15–17], spontaneous emission engineering [18, 19], and optical nonlinearity design [20]. Offering the advantage of extremely high nanorod density ($\sim 10^{10} \text{ cm}^{-3}$), the plasmonic nanorod metamaterial is an ideal platform for the construction of large arrays of tunnel junctions or, upon further structuring [21], nanoscale devices, where guided modes are directly excited by the electron tunneling. Here, we demonstrate

broadband light sources with engineered spectral characteristics, which can be tuned through the visible and infrared spectral ranges and used in integrated devices as well as free-space radiating nanoscale light sources.

2 Experimental and simulation methods

Gold nanorod metamaterials were fabricated by electro-deposition of gold into porous alumina templates on a silica substrate [22], resulting in high-density nanorods oriented perpendicularly to the substrate. In this work, a metamaterial with nanorod average diameter, spacing, and length of around 65 nm, 105 nm, and 480 nm, respectively, was employed (Figure 1A). The spacing between the nanorods is considerably smaller than the wavelength of light, and the nanorod array behaves as an optically uniform medium with optical constants described by the effective medium theory (Figure 1B) [23].

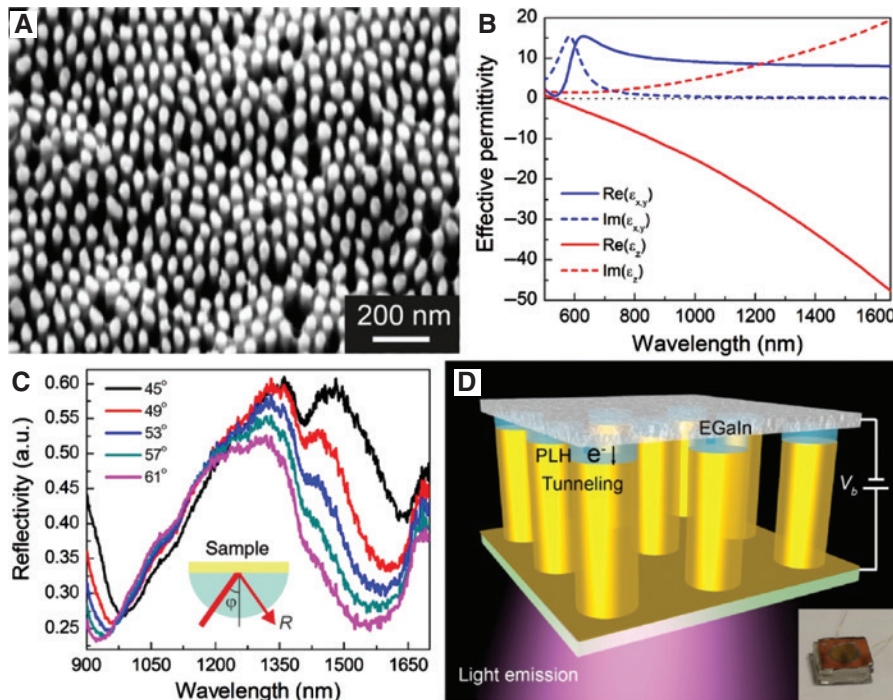


Figure 1: Plasmonic nanorod metamaterial.

(A) Tilted scanning electron microscopy image of a gold nanorod metamaterial with average nanorod spacing of 105 ± 11 nm, nanorod diameter of 65 ± 7 nm, and length of 480 ± 20 nm. (B) Components of the effective permittivity tensor for the gold nanorod metamaterial for light polarization across (x, y) and along (z) the nanorods, calculated using the local effective medium theory. (C) Reflection spectra of the metamaterial tunnel junctions measured from the substrate side in the ATR geometry for different angles of incidence for p -polarized light. (D) Schematic of an electrically driven plasmonic nanorod metamaterial: the tips of the nanorods are separated from a top EGaln electrode with a single-molecule layer of PLH, which creates a tunnel junction. Inset: a photograph of the tunneling device based on the metamaterial shown in (A).

A layer of such a metamaterial acts as a waveguide with the dispersion determined by the metamaterial parameters and the layer thickness [24]. The position of the supported modes can be determined from the minima of the metamaterial reflectivity measured in the attenuated total internal reflection (ATR) configuration (Figure 1C). The tunnel junctions required for the electric excitation of plasmons on the nanorods were constructed at the top of the nanorods by firstly chemical etching the metamaterial to expose the nanorod tips, then functionalizing the exposed parts with a monolayer of poly-L-histidine (PLH) as a dielectric spacer of approximately 1.7 nm, and finally coating them with a droplet of eutectic gallium indium (EGaIn) as a top electrode (see ref. [12] for details).

To model the tunneling-induced emission from the nanorod metamaterial finite element numerical simulations in the frequency domain were performed. As it is commonly done in analytical calculations and numerical simulations, the tunneling current was represented by a dipolar source [25–27]. The point current dipole was placed in the central tunnel junction of a 9×9 square nanorod array, while perfectly matched layers were set on the external domain boundaries to avoid back-reflection from the metamaterial array sides and the substrate. A single dipole was used to represent the non-correlated character of the tunneling events in the array of tunnel junctions, as opposed to the case of the dipoles at each junction, that would represent coherent emission effects, with related phase effects coming into play (in the experiment, the array of the dipoles incoherently radiates into all metamaterial slab modes). The lateral position of the dipole across the nanorod tip was varied; however, as no essential dependence of the output spectrum was observed, a characteristic off-axis position of the dipole $r/\sqrt{2}$ from the nanorod axis was chosen for further simulations (the position at the nanorod axis will discriminate the excitation of asymmetric modes). The size of the array was chosen to be large enough such that it effectively emulates the laterally infinite metamaterial layer. The output power was integrated over a plane positioned 150 nm into the substrate with high numerical aperture (NA), representing the experimental case. Tabulated values were taken for optical properties of gold [28], with an additional mean free path correction of 3 nm [29], representing the granulated nature of the electrodeposited gold, which was determined to be appropriate in previous studies [30]. The optical properties of EGaIn, SiO₂, and Al₂O₃ were approximated by the Drude model (with high-frequency optical constant $\epsilon_\infty = 1.08$, plasma frequency $\omega_p = 13.5$ eV, and scattering rate $\gamma = 1.05$ eV) [31] and Sellmeier models [32, 33], respectively, while tabulated data were taken for T₂O₅ [34].

3 Results and discussion

Upon the application of an electric bias between the top electrode and the nanorods, electrons tunnel through the nanoscale junctions, which can be clearly seen in the characteristic non-linear current-voltage (I - V) curve of the device (Figure 2A). Due to the small diameter of the nanorods and their sharp rims, the efficiency of the electron tunneling is relatively high compared to a smooth film, as the electron momentum relaxation is achieved at the nanorod tips for the electrons with a broader angular distribution of momenta, which otherwise would be reflected at the interface of a smooth film. During the tunneling process, the majority of electrons tunnel elastically with conservation of their energy, appearing as hot electrons in the nanorods, while the remaining electrons tunnel inelastically, losing their energy to excite the plasmonic modes of the metamaterial device (Figure 2B). In this way, the excitation of the modes of the metamaterial slab is achieved, which can be either waveguided or Fabry-Perot modes. These modes can then couple to light and lead to the free-space emission. The device shows strong light generation throughout the visible and near-infrared spectral ranges, depending on the applied bias (Figure 2C). For low biases, the radiation is primarily in the near-infrared as the high-frequency spectrum cutoff is determined by $\hbar\omega_c = eV_b$ and the intensity is also relatively low due to the decreased spectral density of tunneling current near the cutoff. With the increase of the applied bias, there is a rise in the overall emission intensity together with a gradual relative increase of the emission in the shorter wavelength range. The spectrum weakly depends on the emission angle in the ATR geometry and is similar for both s - and p -polarized components of the out-coupled light (Figure 2D, E). The emission from the electrically driven devices reveals good operation stability, as was shown previously [12]. Due to the high reproducibility in the control of the structural parameters (nanorod diameter, spacing, and length as well as the tunneling gap thickness) that define the optical density of states, similar emission spectra are observed for devices with similar structural parameters.

The spectrum of the emission in Figure 2C is determined by $I(\omega) \propto \hbar\omega\Gamma_{e-p}(\omega, V_b)\eta_{\text{rad}}$, where $\Gamma_{e-p}(\omega, V_b)$ is the inelastic tunneling rate and η_{rad} is the efficiency of coupling of the metamaterial modes to the free-space radiation. The inelastic tunneling rate $\Gamma_{e-p}(\omega, V_b) \propto C(\omega, V_b)\rho_{\text{LDOS}}(\omega)$ depends on the emission power spectrum of the fluctuating tunneling current $C(\omega, V_b)$ and the local density of the electromagnetic states $\rho_{\text{LDOS}}(\omega)$ [26, 35]. The power spectrum $C(\omega, V_b) \propto (1 - \hbar\omega/eV_b)$ is determined by the matrix

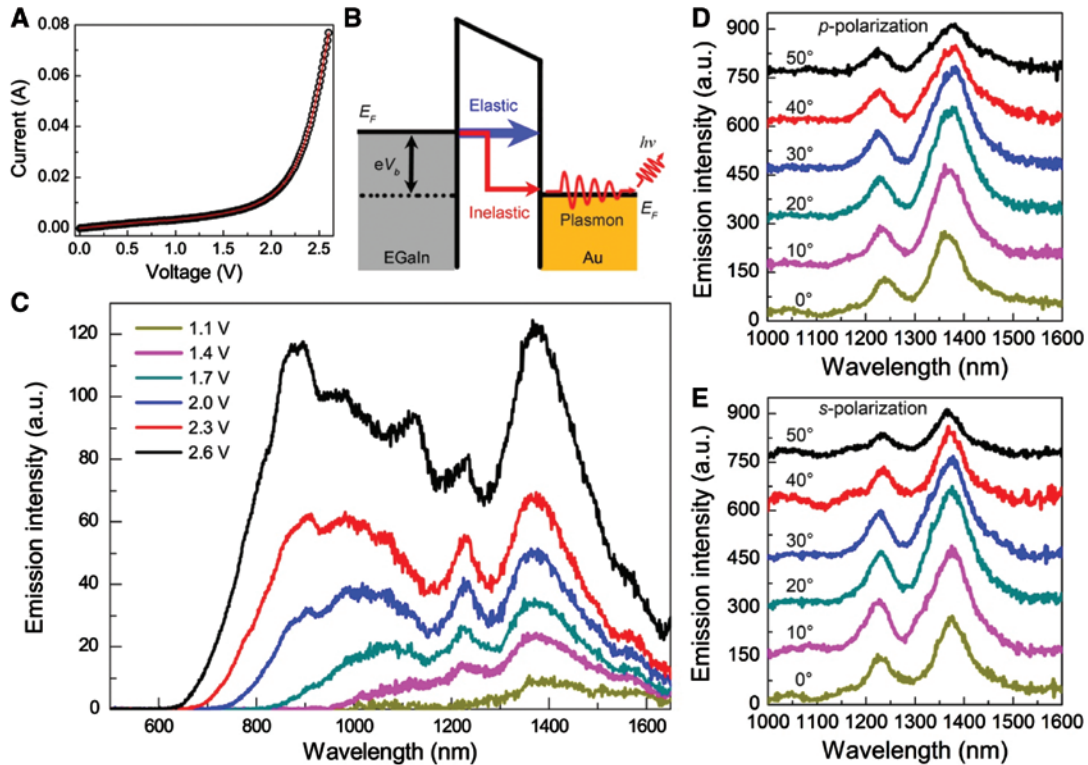


Figure 2: Tunneling-induced optical emission from plasmonic nanorod metamaterials.

(A) Experimentally measured I - V characteristic of the device. (B) Schematic of the tunneling process showing both elastic and inelastic tunneling pathways; the latter results in the excitation of plasmonic modes in the nanorod metamaterial and the consequent emission of light. (C) Experimental emission spectra for various biases measured at normal to the substrate using an objective with $NA=0.4$. (D, E) Experimentally measured emission spectra of the tunneling device for (D) p -polarized and (E) s -polarized light in the ATR configurations for different angles of observation φ under the bias of 1.5 V. The metamaterial parameters are the same as in Figure 1A.

element of the inelastic (accompanied by the generation of an electromagnetic quantum) transition from an electronic state in one electrode to its counterpart in another [25–27]. The shift of generated photons to the shorter wavelength in the observed spectra with the increase of the bias V_b (Figure 2C) is driven by the corresponding evolution of the tunneling current power spectrum $C(\omega, V_b)$. The spectral profile of the emission is shaped by the local density of electromagnetic states $\rho_{\text{LDOS}}(\omega)$, defined by the spectrum of the electromagnetic modes supported by the metamaterial device, while the final spectral dependence measured in the far field is additionally influenced by the coupling efficiency of these modes to the free-space radiation η_{rad} .

The free-space emission from the tunneling current takes place through the excitation of the metamaterial modes (defining the local density of states at the location of the tunneling current), which subsequently radiate into the substrate with certain efficiency η_{rad} . The modal structure of the metamaterial tunneling device was probed by a standard approach based on the study of the metamaterial slab reflectivity. As can be seen from the comparison

of the emission spectrum and the reflectivity at various angles of incidence (Figure 3A, C), the peaks of the emission are in excellent agreement with the reflectivity dips, corresponding to the excitation of the modes of the metamaterial device. Good agreement can also be seen in the nature and structure of the modes and the field distribution produced by the tunneling electrons (c.f. Figure 3B and D). The modes of the tunneling device can be separated into two types: waveguided and Fabry-Perot modes of the metamaterial slab and a localized fundamental MIM mode supported by the tunneling gap (Figure 3). The distributions of the emission field confirm their origin and classification (c.f. Figure 3B and D). They clearly affect the emission spectra of the tunneling device. The efficiency of the inelastic tunneling process resulting in the emission into the waveguided or MIM modes (depending on the wavelength) was estimated to be around 0.1% [12], which is in agreement with previous experimental observations. Further multiplication by $\eta_{\text{rad}} \sim 0.001$ gives the conversion efficiency into the emitted photons (the ratio between the number of emitted photons and the number of tunneled electrons).

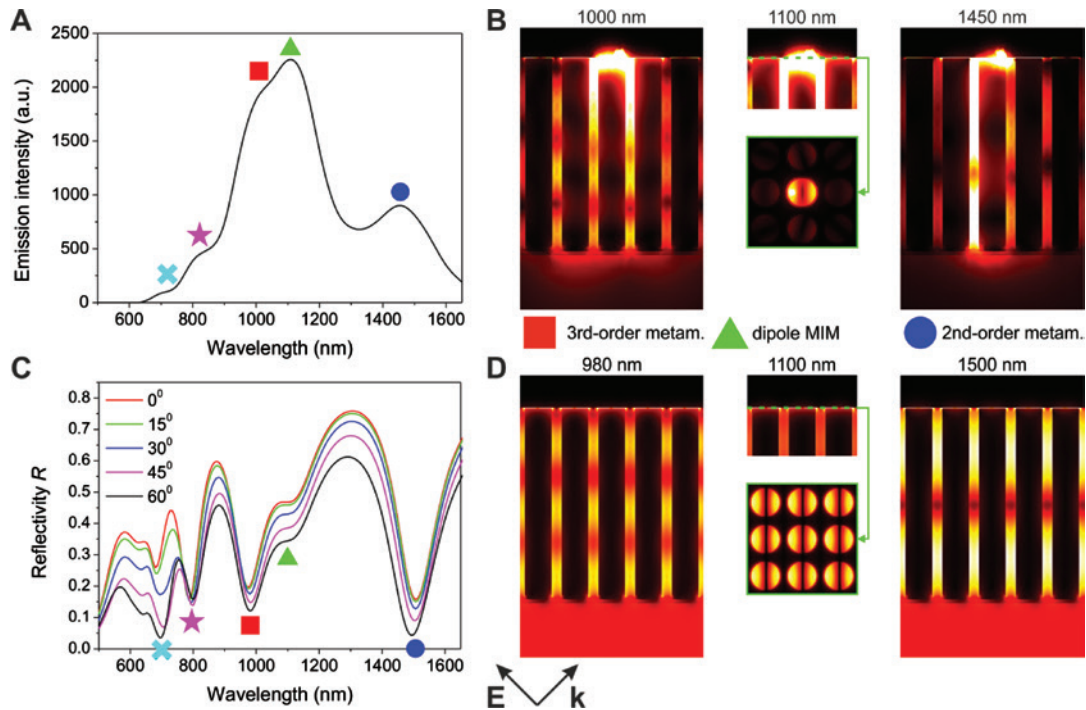


Figure 3: Numerical simulations of the metamaterial modes.

(A) Emission spectrum of the nanorod metamaterial under the bias of 2.6 V collected at an angular range defined by the experimental NA at normal direction. (B) The maps of the electric field norm $|E|$ for the optical modes [marked in (A)] excited by the electron tunneling in one nanorod in the metamaterial (in the experiment, the total field will be an incoherent sum of emission intensities from the tunneling currents of all nanorods of the metamaterial). (C) ATR spectra simulated for the metamaterial device in (A) at various angles of incidence of p -polarized light (the angles are measured in the substrate). The reflection minima correspond to the modes of the device: (circle) second-, (square) third-, (star) fourth-, and (cross) fifth-order modes of the metamaterial slab and (triangle) fundamental MIM mode of the tunneling gap formed by the nanorod/PLH polymer/EGaIn structure. (D) The maps of the electric field norm $|E|$ for the metamaterial modes [marked in (C)] excited by plane wave illumination through the substrate at the incident angle of 45°. Please note that the dielectric layer in the MIM waveguide is 1.7 nm, which corresponds to the thin field enhancement region at the top of the nanorods in the cross-sectional plots. The geometrical parameters for the simulations (s, d, l) = (96, 71, 500) nm were found from the best fit to the experimental ATR spectra.

It is particularly important to stress here that the dipolar-type source related to the tunneling current possesses a wide range of in-plane wavevectors. Therefore, it can couple to all metamaterial modes with various in-plane wavevectors. A subset of this range, defined by the NA of the objective and ATR geometry, after coupling to the free-space radiation, will be detected as the emission signal in the experiment.

The modes of the metamaterial tunneling device are weakly dispersive (Figure 4), resulting in the weak dependence of the emission spectra on the angle of detection and polarization of the detected light and, therefore, well-pronounced peaks in the emission spectrum (Figure 3A) present the superposition of the emission into MIM and p -polarized modes (Figure 4A) and s -polarized modes (Figure 4B). It should be noted that the modes of the metamaterial slab alone, without the tunneling gap and the EGaIn electrode (in the absence of the MIM mode), when the fields of the metamaterial

modes significantly penetrate the superstrate, regain their dispersive nature, as was previously observed [24]. The simulated mode structure is in agreement with that experimentally measured in Figure 1C; however, a more complex mode structure at around 1500-nm wavelength is observed in the experiment. Generally, the angle-resolved emission spectra and angle-resolved reflection measurements present a similar probe of the mode structure of the device. It should be noted that the spectral widths of the modes are rather large, and the waveguided and MIM modes spectrally overlap. Thus, although the predominant character of the mode corresponding to each dip is clear, the modes may have a hybrid MIM/metamaterial nature. In particular, the third-order mode of the metamaterial slab and the fundamental MIM mode appear to overlap so that the energy can be efficiently channeled to the opposite side of the metamaterial, and as the result the strongest emission intensity is observed at the wavelength of these modes (Figure 3A).

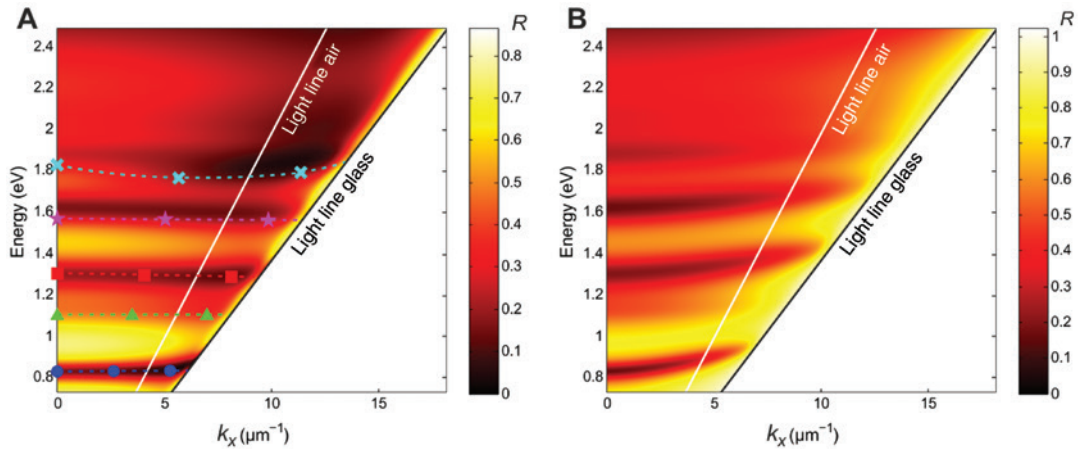


Figure 4: Dispersion of the metamaterial modes.

Dispersion of (A) p -polarized and (B) s -polarized modes supported by the metamaterial device, obtained in the numerical simulations of the reflection. Light lines in the air and the substrate are shown. The mode notations in (A) and the metamaterial device parameters are the same as in Figure 3.

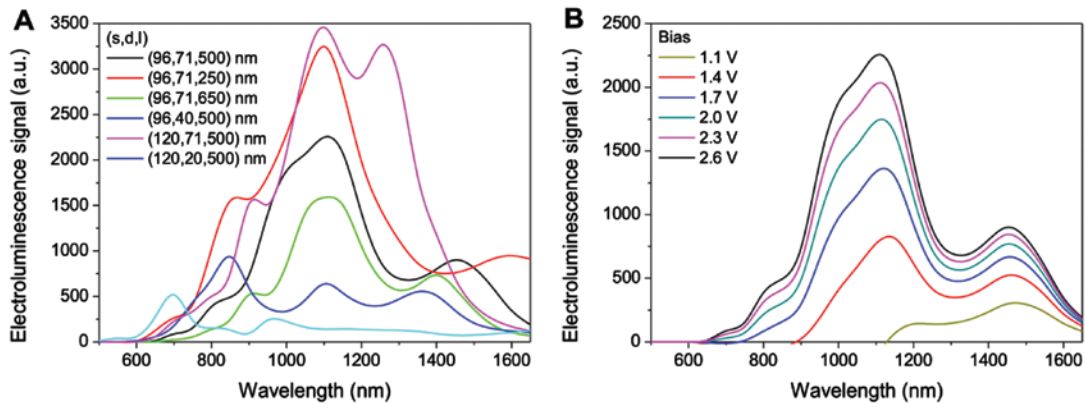


Figure 5: Tuning the metamaterial emission spectrum.

(A) Emission spectra of the metamaterial under the bias of 2.6 V for various geometrical parameters of the metamaterial (s – separation, d – diameter, and l – length of the nanorods in the metamaterial). (B) Emission spectra of the metamaterial under the various biases for the metamaterial with the geometrical parameters $(s, d, l) = (96, 71, 500)$ nm. In both plots, the emission is detected normally to the metamaterial slab with an angle range defined by the experimental NA.

From the practical point of view, electrically driven metamaterials present a flexible platform that can be tuned to target particular applications. Their material components can be varied and the geometrical parameters can be tuned in a wide range during the fabrication process [36]. This gives the opportunity to engineer the modal structure of the metamaterial layer and the tunneling gap, and through them to control the tunneling emission spectrum. The emission spectra obtained with various metamaterial structures illustrate the flexibility of the metamaterial platform to design the emission spectrum in a wavelength range from 700 to 1600 nm through the modification of the spectrum of the supported metamaterial modes with the practically feasible geometrical parameters (Figure 5A). Furthermore, as was also seen

in the experiment (Figure 2C), the emission spectrum can be tuned in the same spectral range by varying the applied bias (Figure 5B). This allows the development of integrated photonic sources for a great variety of waveguide platforms, including Si, plasmonic, or polymer waveguides, to which coupling from the metamaterial waveguided modes and required spectral range can be appropriately designed.

4 Conclusion

We demonstrated a flexible electrically driven nanorod metamaterial platform for the realization of integrated

and free-space electrically driven nanoscale light sources. The tunneling current through a polymer gap between an array of vertically oriented nanorods locally excites the metamaterial plasmonic modes, which, upon outcoupling to photons, create free-space emission. The spectrum of the emission is defined by the structure of the metamaterial device modes, which were identified as waveguided and Fabry-Perot modes of the metamaterial slab of various orders and a dipolar MIM mode localized in the tunneling gap. The modes and, therefore, the emission spectrum in the visible and near-infrared spectral ranges, can be robustly engineered through the control of the effective optical properties of the metamaterial by defining its geometrical parameters at the fabrication step. Such nanoscale light sources are important for the development of integrated nanophotonics, imaging, metrology, and optical sensing platforms.

Acknowledgments: This work was funded, in part, by the Engineering and Physical Sciences Research Council (UK) and the European Research Council iPLASMM project (321268).

References

- [1] Lal S, Link S, Halas NJ. Nano-optics from sensing to waveguiding. *Nat Photonics* 2007;1:641–8.
- [2] Zayats AV, Smolyaninov II, Maradudin AA. Nano-optics of surface plasmon polaritons. *Phys Rep* 2005;408:131–314.
- [3] Xia F, Wang H, Xiao D, Dubey M, Ramasubramaniam A. Two-dimensional material nanophotonics. *Nat Photonics* 2014;8:899–907.
- [4] Park H, Fang AW, Kodama S, Bowers JE. Hybrid silicon evanescent laser fabricated with a silicon waveguide and III-V offset quantum well. *Opt Express* 2005;13:9460–4.
- [5] Guang-Hua D, Jany C, Le Liepvre A, et al. Hybrid III-V on silicon lasers for photonic integrated circuits on silicon. *IEEE J Select Top Quant Elect* 2014;20:158–70.
- [6] McPolin CPT, Bouillard JS, Vilain S, et al. Integrated plasmonic circuitry on a vertical-cavity surface-emitting semiconductor laser platform. *Nat Commun* 2016;7:12409.
- [7] Ma RM, Oulton RF. Applications of nanolasers. *Nat Nanotechnol* 2019;14:12–22.
- [8] Huang KCY, Seo M-K, Sarmiento T, Huo Y, Harris JS, Brongersma ML. Electrically driven subwavelength optical nanocircuits. *Nat Photonics* 2014;8:244–9.
- [9] Smolyaninov II, Khaikin MS, Edelman VS. Light-emission from the tunneling junction of the scanning tunneling microscope. *Phys Lett A* 1990;149:410–2.
- [10] Kern J, Kullock R, Prangsa J, Emmerling M, Kamp M, Hecht B. Electrically driven optical antennas. *Nat Photonics* 2015;9:582–6.
- [11] Du W, Wang T, Chu HS, Nijhuis CA. Highly efficient on-chip direct electronic-plasmonic transducers. *Nat Photonics* 2017;11:623–7.
- [12] Wang P, Krasavin AV, Nasir ME, Dickson W, Zayats AV. Reactive tunnel junctions in electrically driven plasmonic nanorod metamaterials. *Nat Nanotechnol* 2018;13:159–65.
- [13] Qian HL, Hsu SW, Gurunatha K, et al. Efficient light generation from enhanced inelastic electron tunnelling. *Nat Photonics* 2018;12:485–9.
- [14] Wang P, Nasir ME, Krasavin AV, Dickson W, Zayats AV. Multi-level nonvolatile optoelectronic memory based on memristive plasmonic tunnel junctions. Available at: <https://arxiv.org/abs/1811.03347> 2018.
- [15] Wang P, Nasir ME, Krasavin AV, Dickson W, Jiang YL, Zayats AV. Plasmonic metamaterials for nanochemistry and sensing. *Acc Chem Res* 2019;52:3018–28.
- [16] Kabashin AV, Evans P, Pastkovsky S, et al. Plasmonic nanorod metamaterials for biosensing. *Nat Mater* 2009;8:867–71.
- [17] Nasir ME, Dickson W, Wurtz GA, Wardley WP, Zayats AV. Hydrogen detected by the naked eye: optical hydrogen gas sensors based on core/shell plasmonic nanorod metamaterials. *Adv Mater* 2014;26:3532–7.
- [18] Roth DJ, Krasavin AV, Wade A, et al. Spontaneous emission inside a hyperbolic metamaterial waveguide. *ACS Photonics* 2017;4:2513–21.
- [19] Ginzburg P, Roth DJ, Nasir ME, et al. Spontaneous emission in non-local materials. *Light Sci Appl* 2017;6:e16273.
- [20] Neira AD, Olivier N, Nasir ME, Dickson W, Wurtz GA, Zayats AV. Eliminating material constraints for nonlinearity with plasmonic metamaterials. *Nat Commun* 2015;6:7757.
- [21] Dickson W, Beckett S, McClatchey C, et al. Hyperbolic polaritonic crystals based on nanostructured nanorod metamaterials. *Adv Mater* 2015;27:5974–80.
- [22] Evans P, Hendren WR, Atkinson R, et al. Growth and properties of gold and nickel nanorods in thin film alumina. *Nanotechnology* 2006;17:5746–53.
- [23] Elser J, Wangberg R, Podolskiy VA, Narimanov EE. Nanowire metamaterials with extreme optical anisotropy. *Appl Phys Lett* 2006;89:261102.
- [24] Vasilantonakis N, Nasir ME, Dickson W, Wurtz GA, Zayats AV. Bulk plasmon-polaritons in hyperbolic nanorod metamaterial waveguides. *Laser Photon Rev* 2015;9:345–53.
- [25] Rendell RW, Scalapino DJ. Surface plasmons confined by microstructures on tunnel junctions. *Phys Rev B* 1981;24:3276–94.
- [26] Persson BN, Baratoff A. Theory of photon emission in electron tunneling to metallic particles. *Phys Rev Lett* 1992;68:3224–7.
- [27] Johansson P. Light emission from a scanning tunneling microscope: fully retarded calculation. *Phys Rev B* 1998;58:10823–34.
- [28] Johnson PB, Christy RW. Optical constants of the noble metals. *Phys Rev B* 1972;6:4370–9.
- [29] Lissberger PH, Nelson RG. Optical-properties of thin-film Au-MgF₂ cermets. *Thin Solid Films* 1974;21:159–72.
- [30] Pollard RJ, Murphy A, Hendren WR, et al. Optical nonlocalities and additional waves in epsilon-near-zero metamaterials. *Phys Rev Lett* 2009;102:127405.
- [31] Blaber MG, Engel CJ, Vivekchand SR, Lubin SM, Odom TW, Schatz GC. Eutectic liquid alloys for plasmonics: theory and experiment. *Nano Lett* 2012;12:5275–80.

- [32] Malitson IH. Interspecimen comparison of refractive index of fused silica. *J Opt Soc Am* 1965;55:1205–8.
- [33] Malitson IH, Dodge MJ. Refractive-index and birefringence of synthetic sapphire. *J Opt Soc Am* 1972;62:1405.
- [34] Gao LH, Lemarchand F, Lequime M. Exploitation of multiple incidences spectrometric measurements for thin film reverse engineering. *Opt Express* 2012;20:15734–51.
- [35] Parzefall M, Bharadwaj P, Jain A, Taniguchi T, Watanabe K, Novotny L. Antenna-coupled photon emission from hexagonal boron nitride tunnel junctions. *Nat Nanotechnol* 2015;10:1058–63.
- [36] Nasir ME, Peruch S, Vasilantonakis N, et al. Tuning the effective plasma frequency of nanorod metamaterials from visible to telecom wavelengths. *Appl Phys Lett* 2015;107:121110.